DOI: 10.1002/anie.201204792

Ferroelectric Nanoplates

Self-Templated Synthesis of Single-Crystal and Single-Domain Ferroelectric Nanoplates**

Chunying Chao, Zhaohui Ren, Yihan Zhu, Zhen Xiao, Zhenya Liu, Gang Xu, Jiangquan Mai, Xiang Li, Ge Shen, and Gaorong Han**

Low-dimensional nanomaterials, such as nanowires[1] and nanotubes,[2,3] have received extensive attention because of their fascinating catalysis,[4] optics,[5] and electronics[6,7] properties, which offer the opportunity to fabricate nanodevices. Much attention has been paid to materials with two-dimensional (2D) nanostructure because of their unique electronic, magnetic, and storage properties.[8–10] In particular, the recent development of stable graphene has stimulated great interest in studying free-standing 2D nanomaterials.[8] So far, a variety of 2D free-standing materials with nanostructure, such as PbS nanosheets,[9] WO_3 nanoplates,[10] CeO_2 nanoplates,[11] MoS_2 nanoflakes,[12,13] and TiO_2 nanosheets,[4] have been successfully synthesized. Compared to these simple compounds, 2D free-standing, single-crystal multicomponent oxide nanomaterials, such as ferroelectric oxides, have been rarely reported because of the relatively complex crystal structures and rigid crystalline properties of these oxides.

Ferroelectric oxide nanomaterials, such as $PbTiO_3$ (PT), $Pb(Zr,Ti)O_3$, and $BaTiO_3$, have versatile properties for various technical applications ranging from nonvolatile ferroelectric random access memories (NFERAMs) to electromechanical applications.[14,15] Among these nanomaterials, 2D free-standing, single-crystal ferroelectric materials are highly attractive because of their potential performances. For example, ultrathin single crystals of $BaTiO_3$[16,17] prepared by focused ion beam (FIB) microscopy have been used as single-crystal capacitors with thicknesses down to about 65 nm. These ferroelectric platelets fabricated by FIB have greatly improved our understanding of the fundamental properties of thin films.[18,19] However, recent theoretical research predicts that ferroelectric nanodiscs could even favor an ultimate NFERAM density of 60×10^{12} bits per square inch as well as a new toroid moment.[20] In contrast to the conventional properties, the surface chemistry of ferroelectric oxides only gradually became an active field of research.[21] In particular, it has been predicted that CO and NO catalysis could be favored on ultrathin Pt(100) films supported on ferroelectric $PbTiO_3$.[22]

Various methods have so far been applied to fabricate 0D and 1D ferroelectric nanomaterials, including templated methods,[23–26] sol-gel processing,[27,28] soft-chemistry routes,[29] solvothermal/hydrothermal reactions,[30,31] and electrospinning techniques.[32,33] Despite much effort, there is still an absence of a simple wet-chemistry method to prepare 2D single-crystal ferroelectric nanomaterials, such as nanoplates and nanodiscs. Here we report, for the first time, that free-standing, single-crystal PT nanoplates can be synthesized by a facile hydrothermal method. The characterization of the microstructure by X-ray diffraction (XRD) and high-resolution transmission electron microscopy (HRTEM) demonstrates that these PT nanoplates, with side lengths of 600–1100 nm and heights of about 150 nm, grow along the *ab* plane of the tetragonal perovskite structure and that {001} facets at the top and bottom surfaces are exposed. The "self-templated" crystal growth has been employed to discuss the mechanism for the formation of PT nanoplates under hydrothermal conditions. Electrostatic force microscopy in the dynamic contact mode (DC-EFM) of operation was also used to study the ferroelectric properties of the PT nonaplates. Furthermore, the catalytic performance of the nanoplates for the oxidation of carbon monoxide (CO) has been evaluated.

In brief, tetragonal-phase PT nanoplates were synthesized by a hydrothermal method at 200 °C by using 6 M KOH. Figure 1 a shows a typical XRD pattern (JCPDS 70-0746) of PT nanoplates prepared by the hydrothermal process at 200 °C for 12 h with 6 M KOH, and indicates that the product has a pure tetragonal perovskite PT structure. More importantly, the intensity of the (001) diffraction peak is dramatically higher than that of (100), which is opposite to the case in conventional perovskite PT (JCPDS 70-0746). This observation reveals that {001} crystal planes are prevailent in the sample. Scanning electron microscopy (SEM) and TEM analysis show that the products consist of well-defined structures with a rectangular outline and a side length of 600–1100 nm (Figure 1 b,c). The HRTEM image (Figure 1 d) of a PT nanoplate shows a clear crystal lattice with uniform interplanar spacings of 0.390 nm and 0.390 nm, which correspond to the tetragonal (100) and (010) planes, respectively, and indicate that the PT nanoplates grow along the *ab* plane of the perovskite structure. The effect of the KOH concen-

[*] C. Y. Chao, Dr. Z. H. Ren, Z. Xiao, Z. Y. Liu, Dr. G. Xu, J. Q. Mai, Dr. X. Li, Dr. G. Shen, Dr. G. R. Han
State Key Laboratory of Silicon Materials
Department of Materials Science and Engineering
Cyrus Tang Center for Sensor Materials and Application
Zhejiang University, Hangzhou 310027 (P.R. China)
E-mail: renzh@zju.edu.cn
hgr@zju.edu.cn
Dr. Y. H. Zhu
Advanced Membranes and Porous Materials Center
King Abdullah University (Saudi Arabia)

[**] This work was financially supported by the National Natural Science Foundation of China (No.51102212), the Fundamental Research Funds for the Central Universities (no. 588040*172210221/014), and the Opening Foundation of Zhejiang Provincial Top Key Discipline.

Supporting information for this article is available on the WWW under http://dx.doi.org/10.1002/anie.201204792.

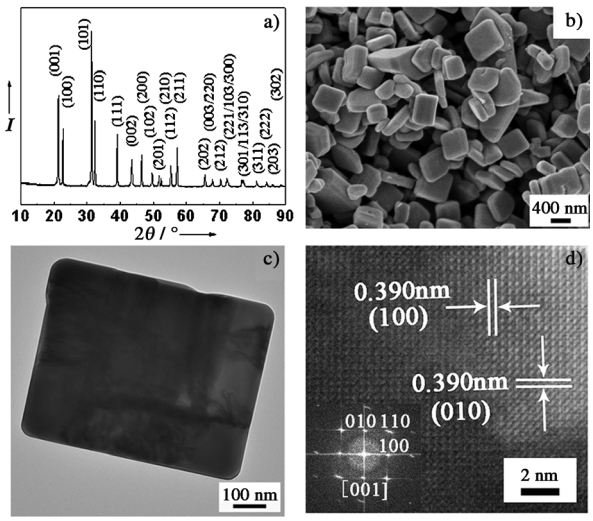

Figure 1. a) Typical XRD pattern and b) SEM image of PT nanoplates synthesized hydrothermally at 200 °C for 12 h. c) Low-magnification TEM image of an individual PT nanoplate. d) HRTEM image of an individual PT nanoplate; the inset shows the corresponding fast Fourier transform (FFT) ED pattern along the [001] zone axis.

tration on the formation of free-standing, single-crystal PT nanoplates has also been investigated (see Figure S1 in the Supporting Information).

The topography and domain images of the PT nanoplates was investigated by DC-EFM.[34] NSC15 Ti-Pt cantilevers with a force constant of 5.5 N m^{-1} and a resonance frequency of 160 kHz were used. Figure 2 displays the topographic image, line profiles, and domain contrast of the PT nanoplates observed by DC-EFM. Figure 2 a,b shows that individual PT nanoplates possess a plate-shaped structure and a relatively smooth surface. The height and the lateral size of the PT nanoplates have been determined to be approximately 150 nm and 950–1100 nm, respectively. Figure 2 c shows the topography of three PT nanoplates, while Figure 2 d shows the corresponding domain contrast of the PT nanoplates. The topographic and domain contrast images were obtained simultaneously by DC-EFM. A huge difference—dark and bright regions—can be observed in the domain contrast images. The charge-density image distinctly shows two levels of dark and bright regions that correspond to the positively and negatively polarized domains,[34] respectively, which indicates that the PT nanoplates are single-domain ferroelectric nanoplates. Furthermore, the positively and negatively polarized domains (500 nm × 500 nm) were centered where the DC-EFM tip was positioned on a PT nanoplate during writing, which clearly demonstrates that the PT nanoplates have potential in ferroelectric memory devices (see Figure S2 in the Supporting Information).

The evolution of the crystal structures and morphologies of the products synthesized at 200 °C in 6 M KOH for different periods of times was studied (see Figure S3 in the Supporting Information). When the products were prepared at 200 °C for 20 and 30 minutes, large-scale thin nanoplates and nanoparticles were synthesized, respectively. A prolonged synthesis led to a gradual increase in the thick nanoplates at the expense of the thin nanoplates and nanoparticles. To understand the growth mechanism of the PT nanoplates we focused on the product synthesized hydrothermally at 200 °C for 0.5 h. Figure 3 depicts a comparison of the as-prepared product before and after the acid-washing procedure. Before acid washing (Figure 3 a,b), the product consists of TiO_2 (JCPDS 21-1236), Pb_3O_4 (JCPS 41-1493), and tetragonal PT (JCPDS 70-0746), with large-scale thin nanoplates and nanoparticles being observed (Figure 3 b). Some nanoparticles are absorbed on the surfaces of the thin nanoplates. Moreover, Pb, Ti, and O were detected in the product in a Pb/Ti/O molar ratio of

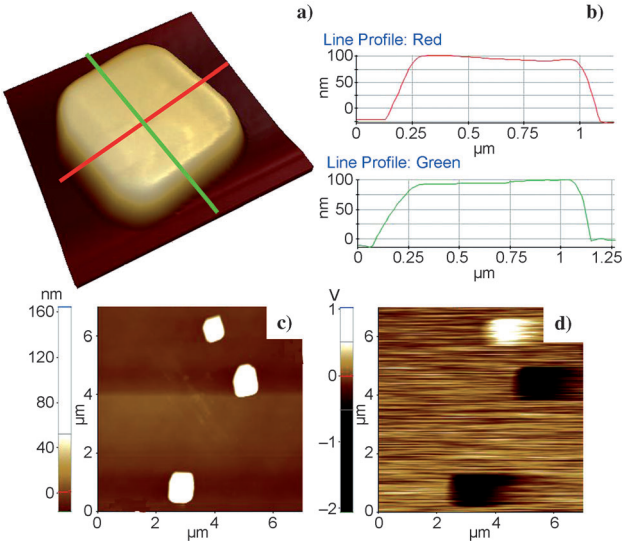

Figure 2. a) DC-EFM topographic image of a PT nanoplate in three dimensions. b) Line profiles of the former PT nanoplate. c) Topographic image and d) domain contrast of three PT nanoplates obtained by DC-EFM.

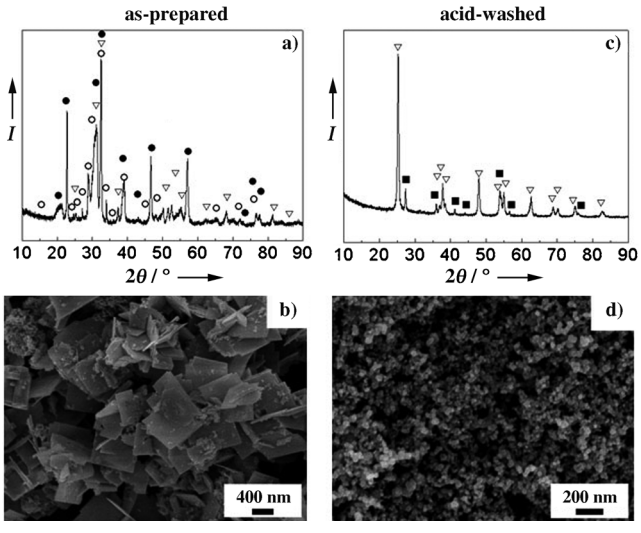

Figure 3. Typical XRD patterns (a,c) and SEM images (b,d) of as-prepared products synthesized at 200 °C for 0.5 h by a hydrothermal process. a,b) As-prepared products; c,d) after acid washing with 1% HNO_3. For (a) ▽ TiO_2 (JCPDS 21-1236), ○ Pb_3O_4 (JCPDS 41-1493), ● $PbTiO_3$ (JCPDS 70-0746); for (c) ▽ anatase TiO_2, ■ rutile TiO_2.

approximate 1:1:3 by energy dispersive spectroscopy (EDS; see Figure S4a in the Supporting Information). After acid washing the product with 1% HNO_3 (Figure 3c,d) only anatase and rutile TiO_2 nanoparticles remain, with a Ti/O molar ratio determined by EDS (Figure S4b) to be close to 1:2. Furthermore, the XRD results were further confirmed by Raman spectroscopy analysis (Figure S4c,d).

The microstructure of the product prepared for 0.5 h has been characterized by high-angle annular dark-field scanning transmission electron microscopy (HAADF STEM) and HRTEM (Figure 4). The HAADF STEM images (Figure 4a)

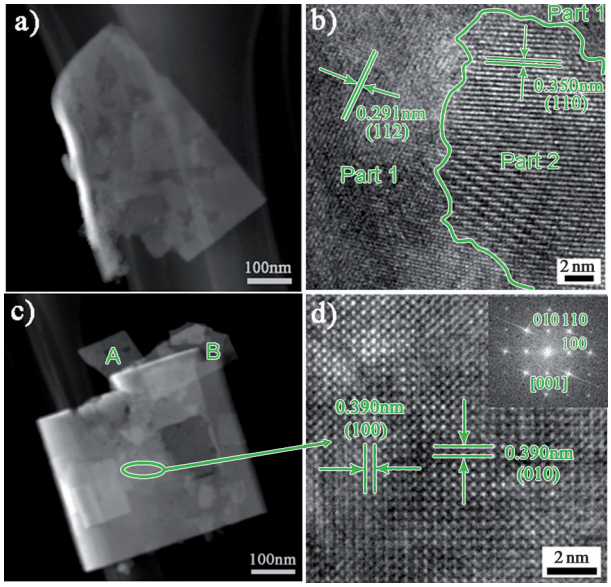

Figure 4. HAADF STEM images of the product synthesized hydrothermally at 200 °C for 0.5 h. a) An individual thin nanoplate. c) A stacked nanoplate. b,d) The corresponding HRTEM images of (a) and (c), the inset in (d) shows the corresponding fast Fourier transform (FFT) ED pattern along the [001] zone axis.

and DC-EFM detection (see Figure S5 in the Supporting Information) show that the individual thin nanoplates usually have side lengths of 400–800 nm and heights of about 22 nm. There are two types of crystal structures in the HRTEM image of the thin nanoplate (Figure 4b). The crystal lattice in Part 1 shows an interplanar spacing of 0.291 nm, which corresponds to the (112) crystalline plane of Pb_3O_4. The crystal lattice in Part 2 reveals that a particle with a size of approximately 18 nm is a single crystal with an interplanar spacing of 0.350 nm, which corresponds to the (110) crystalline plane of TiO_2. Such an observation strongly suggests that TiO_2 nanoparticles are embedded in the Pb_3O_4 thin plate. Interestingly, these thin nanoplates stacked into a thick nanoplate with a side length of 400–800 nm (Figure 4c). Figure 4d shows the HRTEM image of stacked thin nanoplates, which demonstrates a clear crystal lattice with uniform interplanar spacings of 0.390 nm and 0.390 nm, which correspond to the tetragonal (100) and (010) planes, respectively, and indicate that perovskite PT structures are formed. Moreover, the HRTEM images of unstacked thin nanoplates (areas A and B in Figure 4c) are the same as that of the individual thin nanoplates (Figure 4b; see Figure S5 in the Supporting Information). Furthermore, the size of the thick nanoplate is close to that of the PT nanoplates. The PT nanoplate (height of ca. 150 nm, Figure 2b) probably forms by the stack and Ostwald ripening process of 5–7 layers of thin nanoplates (height of ca. 22 nm; see Figure S5 in the Supporting Information). In particular, the negatively polarized domains (Figure S5f) detected in some regions suggested that tetragonal phase PT was formed in these regions within the thin nanoplate. Furthermore, the Pb, Ti, and O mappings (see Figure S6 in the Supporting Information) demonstrate that the Pb, Ti, and O atoms are almost uniformly distributed in the thin nanoplates. However, the Ti mapping shows that the Ti is concentrated only in the bright regions (Figure S6b). A quantitative phase analysis of the products synthesized at 200 °C for different times (0.5 h, 2 h, and 6 h) was carried out using Rietveld refinement analysis on the XRD data (see Table S1 in the Supporting Information). After refinement, the phase compositions of the samples were determined to consist of completely crystallized PT, partially crystallized PT, Pb_3O_4 (JCPDS 41-1493), and TiO_2 (JCPDS 21-1236). The weight fractions of completely crystallized PT gradually increase, and the weight fractions of partially crystallized PT, Pb_3O_4 (JCPDS 41-1493), and TiO_2 (JCPDS 21-1236) gradually decrease at prolonged reaction times (see Table S1 in the Supporting Information).

On the basis of the above results, a growth mechanism of single-crystal PT nanoplates under hydrothermal conditions is proposed (Figure 5). Firstly, lead oxides (Pb_3O_4) are

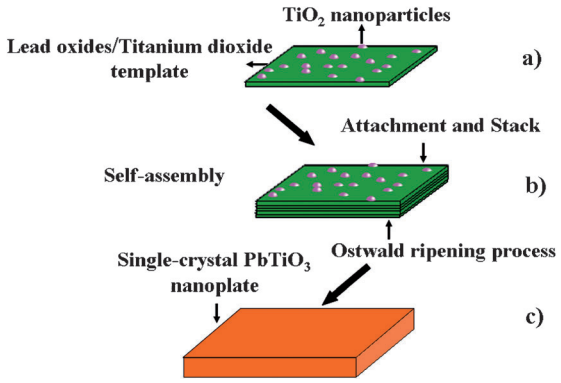

Figure 5. Mechanistic model for the growth of single-crystal $PbTiO_3$ nanoplates prepared under hydrothermal conditions.

produced immediately in the alkaline solution and form the backbone of the nanoplate. TiO_2 particles are then absorbed and embedded within the lead oxide templates, and thin nanoplates are formed (Figure 5a). This stage occurs within a short time (20–30 min) at the reaction temperature (see Figure S3 in the Supporting Information). Thin nanoplates then attach and stack along the vertical direction to the thin nanoplate, a process probably induced by electrostatic forces (Figure 5b). Finally, perovskite-phase PT nanoplates are formed by the surface reconstruction and Ostwald ripening process of thin nanoplates (Figure 5c). Such a process is

supported by a long hold time (1–10 h) and the coexistence of two phases (thin nanoplate and perovskite-phase PT nanoplate; see Figure S3 in the Supporting Information). Moreover, the results confirm that lead oxides play a key role in the formation of the perovskite-phase nanoplates (see Figure S7 in the Supporting Information). When the Pb/Ti molar ratio was set at 1.0:1, the coexistence of only two phases instead of PT nanoplates with a pure perovskite structure was obtained. Hence, the formation of the perovskite PT nanoplates is closely related to the lead oxide/titanium dioxide nanoplates. Therefore, a "self-templated" crystal-growth process under hydrothermal conditions is the dominant mechanism for the formation of the PT nanoplates.

The catalytic activity of ferroelectric PT nanoplates and Pt/PT nanoplates for the oxidation of carbon monoxide (CO) were evaluated as a function of temperature (Figure 6). For

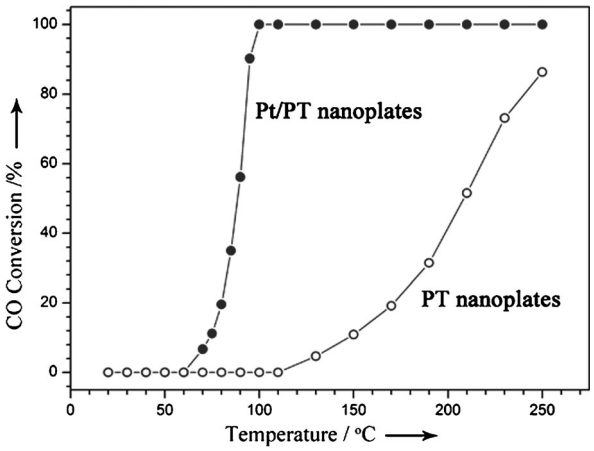

Figure 6. Catalytic activity in terms of carbon monoxide (CO) conversion as a function of reaction temperature.

the pure PT nanoplates, the CO conversion into CO_2 starts around 110 °C and increases slowly up to 250 °C. At least 80 % conversion is observed at 250 °C for the PT nanoplates. However, for the Pt/PT nanoplates, the CO conversion into CO_2 starts around 60 °C and increases significantly from 70 °C to 100 °C, with 100 % conversion occurring at 100 °C (image of a Pt/PT nanoplate shown in Figure S8 in the Supporting Information). In particular, it was found that CO dissociation does not occur on the bulk Pt surface.[24] The BET surface area measurement yielded a value of 1.71 $m^2 g^{-1}$ for PT nanoplates, far lower than that of other oxides.[35–37] Even with such a low surface area, the temperature of the 100 % conversion of CO with the Pt/PT nanoplate system remains lower by at least 40 °C than that of Pt/CeO_2 nanocomposites (the 100 % conversion of CO was 144–223 °C).[35] This finding suggest that a different principle could be involved compared to other oxide catalysts. The ferroelectric polarization of the PT nanoplates may play a crucial role in the CO oxidation, where changes in the molecular potential energy surface are made to the platinum centers to promote the reaction kinetics.[22] Although the catalytic activity was evaluated only for the oxidation of CO in the present study, PT nanoplates or Pt/PT nanoplates could also be effective catalysts for other systems, such as NO_x and automotive exhaust emission.

In summary, we have developed a facile synthetic method to prepare free-standing, single-crystal PT nanoplates. PT nanoplates grow along the *ab* plane of the tetragonal perovskite structure, with exposed {001} facets at the top and bottom surfaces. The PT nanoplates have a side length of 600–1100 nm, a height of about 150 nm, and an aspect ratio of about 6:1. Furthermore, the present findings indicate that PT nanoplates probably form by a "self-templated" crystal-growth process under hydrothermal conditions. More importantly, the PT nanoplates have a ferroelectric single-domain structure, where writing and reading manipulation of the polarization areas within such nanoplates has been realized. Furthermore, the nanoplates could serve as effective catalysts for the oxidation of carbon monoxide (CO). The findings presented here not only provide an opportunity to understand the morphology and size effects on ferroelectricity at the nanoscale but also offer the possibility to explore the catalytic application of ferroelectric oxides, for example, as sensors and in the treatment of automotive exhaust emissions.

Experimental Section

Single-crystal and single-domain PT nanoplates were synthesized by a hydrothermal method as follows: TiO_2 and $Pb(NO_3)_2$ were used as the starting materials. Analytical grade KOH was used as the mineralizer. The Pb/Ti molar ratio was set at 1.25:1 and the concentration of KOH was 6 M. The hydrothermal treatment was performed in an autoclave at 200 °C for different time periods. The resultant products were filtered and washed with 1 % nitric acid, deionized water, and ethanol, and subsequently dried at 60 °C in air for further characterization. The sample was dispersed in ethanol solution, and a drop of solution was dropped onto the Si(100) substrate under ambient conditions until all the ethanol had evaporated. The samples were then analyzed by DC-EFM. The PT nanoplates were dispersed in deionized water in an ultrasonic bath for 30 min. A 0.05 M aqueous solution of chloroplatinic acid ($H_2PtCl_6 \cdot 6H_2O$) was then added to the above suspension. After stirring the mixture for 15 min at room temperature, a 0.2 M solution of $NaBH_4$ (reductant) was added dropwise and the mixture kept in an ultrasonic bath for 30 min. The Pt/PT nanoplates were obtained after centrifugation, washing with deionized water for five times, and then drying at 60 °C for 24 h.

The XRD patterns were obtained on a RIGAKUD-MAX-C with CuKα radiation ($\lambda = 1.54056$ Å). SEM images were collected on a Hitachi field emission SEM MODEL S-4800 equipped with an EDX detector. TEM images were collected on a JEOL JEM-200CX microscope at an accelerating voltage of 160 kV. HRTEM images and high-resolution STEM studies were recorded on a 200 kV FEI F20 transmission electron microscope. DC-EFM was employed to investigate the topography and ferroelectric properties. NSC15 Ti-Pt cantilevers with a force constant of 5.5 $N m^{-1}$ and resonance frequency of 160 kHz were used. The BET surface area of the PT nanoplates was determined from the linear part of the BET isotherm (Brunauer curve in 0.05–0.35 partial pressure range). The ambient pressure CO oxidation model reaction was performed in a continuous flow fixed-bed quartz tubular reactor (6 mm i.d.). 50 mg (40–60 mesh) of a 1 % PT powder or Pt/PT powder catalyst was packed in the reactor and pretreated at 120 °C for 2 h under a dry He flow (50 mL min^{-1}). After cooling the mixture to room temperature, a dry 0.7 vol % CO/33.3 vol % O_2/He mixture feed stock (30 mL min^{-1}) was

introduced into the reactor. All reactants and products were analyzed by on-line gas chromatography.

Received: June 19, 2012
Published online: August 15, 2012

Keywords: ferroelectricity · heterogeneous catalysis · lead titanate · morphology · nanostructures

[1] Y. Xia, P. D. Yang, Y. G. Sun, Y. Y. Wu, B. Mayers, B. Gates, Y. D. Yin, F. Kim, H. Q. Yan, *Adv. Mater.* **2003**, *15*, 353 – 389.
[2] X. H. Zhu, Z. G. Liu, N. B. Ming, *J. Mater. Chem.* **2010**, *20*, 4015 – 4030.
[3] T. Kasuga, M. Hiramatsu, A. Hoson, T. Sekino, K. Niihara, *Adv. Mater.* **1999**, *11*, 1307 – 1311.
[4] X. G. Han, Q. Kuang, M. S. Jin, Z. X. Xie, L. S. Zheng, *J. Am. Chem. Soc.* **2009**, *131*, 3152 – 3153.
[5] A. Tao, P. Sinsermsuksakul, P. Yang, *Nat. Nanotechnol.* **2007**, *2*, 435 – 440.
[6] X. G. Peng, L. Manna, W. D. Yang, J. Wickham, E. Scher, A. Kadavanich, A. P. Alivisatos, *Nature* **2000**, *404*, 59 – 61.
[7] F. X. Redl, K. S. Cho, C. B. Murray, S. O' Brien, *Nature* **2003**, *423*, 968 – 971.
[8] Z. Z. Sun, Z. Yan, J. Yao, E. Beitler, Y. Zhu, J. M. Tour, *Nature* **2010**, *468*, 549 – 552.
[9] C. Schliehe, B. H. Juarez, M. Pelletier, S. Jander, D. Greshnykh, M. Nagel, A. Meyer, S. Foerster, A. Kornowski, C. Klinke, H. Weller, *Science* **2010**, *329*, 550 – 553.
[10] A. Yella, E. Mugnaioli, M. Panthöfer, U. Kolb, W. Tremel, *Angew. Chem.* **2010**, *122*, 3373 – 3377; *Angew. Chem. Int. Ed.* **2010**, *49*, 3301 – 3305.
[11] D. Y. Wang, Y. J. Kang, V. D. Nguyen, J. Chen, R. Küngas, N. L. Wieder, K. Bakhmutsky, R. J. Gorte, C. B. Murray, *Angew. Chem.* **2011**, *123*, 4470 – 4473; *Angew. Chem. Int. Ed.* **2011**, *50*, 4378 – 4381.
[12] R. J. Smith, P. J. King, M. Lotya, C. Wirtz, U. Khan, S. De, A. O. Neill, G. S. Duesberg, J. C. Grunlan, G. Moriarty, J. Chen, J. Z. Wang, A. I. Minett, V. Nicolosi, J. N. Coleman, *Adv. Mater.* **2011**, *23*, 3944 – 3948.
[13] J. N. Coleman, M. Lotya, A. O. Neill, S. D. Bergin, P. J. King, U. Khan, K. Young, A. Gaucher, S. De, R. J. Smith, I. V. Shvets, S. K. Arora, G. Stanton, H. Y. Kim, K. Lee, G. T. Kim, G. S. Duesberg, T. Moriarty, A. Shmeliov, R. J. Nicholls, J. M. Perkins, E. M. Grieveson, K. Theuwissen, D. W. McComb, P. D. Nellist, V. Nicolosi, *Science* **2011**, *331*, 568 – 571.
[14] Y. Kim, H. Kim, W. Lee, M. Alexe, S. Baid, J. K. Kim, *Nano Lett.* **2010**, *10*, 2141 – 2146.
[15] M. Alexe, D. Hesse, *J. Mater. Sci.* **2006**, *41*, 1 – 11.
[16] J. F. Scott, *Science* **2007**, *315*, 954 – 959.
[17] M. M. Saad, P. Baxter, R. M. Bowman, J. M. Gregg, F. D. Morrison, J. F. Scott, *J. Phys. Condens. Matter* **2004**, *16*, L451 – L456.
[18] L. W. Chang, M. McMillen, F. D. Morrison, J. F. Scott, J. M. Gregg, *Appl. Phys. Lett.* **2008**, *93*, 132904.
[19] L. W. Chang, M. Alexe, J. F. Scott, J. M. Gregg, *Adv. Mater.* **2009**, *21*, 4911 – 4914.
[20] I. I. Naumov, L. Bellaiche, H. Fu, *Nature* **2004**, *432*, 737 – 740.
[21] K. Garrity, A. M. Kolpak, S. Ismail-Beigi, E. I. Altman, *Adv. Mater.* **2010**, *22*, 2969 – 2973.
[22] A. M. Kolpak, I. Grinberg, A. M. Rappe, *Phys. Rev. Lett.* **2007**, *98*, 166101.
[23] B. A. Hernandez, K. S. Chang, E. R. Fisher, P. K. Dorhout, *Chem. Mater.* **2002**, *14*, 480 – 482.
[24] S. Kronholz, S. Rathgeber, S. Karthäuser, H. Kohlstedt, S. Clemens, T. Schneller, *Adv. Funct. Mater.* **2006**, *16*, 2346 – 2354.
[25] J. M. Macak, C. Zollfrank, B. J. Rodriguez, H. Tsuchiya, M. Alexe, P. Greil, P. Schmuki, *Adv. Mater.* **2009**, *21*, 3121 – 3125.
[26] N. Nuraje, K. Su, A. Haboosheh, J. Samson, E. P. Manning, N. Yang, H. Matsui, *Adv. Mater.* **2006**, *18*, 807 – 811.
[27] S. O'Brien, L. Brus, C. B. Murray, *J. Am. Chem. Soc.* **2001**, *123*, 12085 – 12086.
[28] J. J. Urban, W. S. Yun, Q. Gu, H. Park, *J. Am. Chem. Soc.* **2002**, *124*, 1186 – 1187.
[29] M. Niederberger, N. Pinna, J. Polleux, M. Antonietti, *Angew. Chem.* **2004**, *116*, 2320 – 2323; *Angew. Chem. Int. Ed.* **2004**, *43*, 2270 – 2273.
[30] D. R. Modeshia, R. I. Walton, *Chem. Soc. Rev.* **2010**, *39*, 4303 – 4325.
[31] Z. H. Ren, G. Xu, Y. Liu, X. Wei, Y. H. Zhu, X. B. Zhang, G. L. Lv, Y. W. Wang, Y. W. Zeng, P. Y. Du, W. J. Weng, G. Shen, J. Z. Jiang, G. R. Han, *J. Am. Chem. Soc.* **2010**, *132*, 5572 – 5573; G. Xu, Z. H. Ren, P. Y. Du, W. J. Weng, G. Shen, G. R. Han, *Adv. Mater.* **2005**, *17*, 907 – 910.
[32] X. F. Lu, D. L. Zhang, Q. D. Zhao, C. Wang, W. J. Zhang, Y. Wei, *Macromol. Rapid Commun.* **2006**, *27*, 76 – 80.
[33] J. F. Scott, H. J. Fan, S. Kawasaki, J. Banks, M. Ivanov, A. Krotkus, J. Macutkevic, R. Blinc, V. V. Laguta, P. Cevc, J. S. Liu, A. L. Kholkin, *Nano Lett.* **2008**, *8*, 4404 – 4409.
[34] J. W. Hong, K. H. Noh, *Phys. Rev. B* **1998**, *58*, 5078 – 5084.
[35] H. P. Zhou, H. S. Wu, J. Shen, A. X. Yin, L. D. Sun, C. H. Yan, *J. Am. Chem. Soc.* **2010**, *132*, 4998 – 4999.
[36] J. A. Enterkin, W. Setthapun, J. W. Elam, S. T. Christensen, F. A. Rabuffetti, L. D. Marks, P. C. Stair, K. R. Poeppelmeier, C. L. Marshall, *ACS Catal.* **2011**, *1*, 629 – 635.
[37] R. N. S. H. Magalhães, F. S. Toniolo, V. T. da Silva, M. Schmal, *Appl. Catal. A* **2010**, *388*, 216 – 224.

